Journal of Semiconductors
(2023) 44, 061802
doi: 10.1088/1674-4926/44/6/061802

REVIEWS

Recent advances in NiO/Ga_2O_3 heterojunctions for power electronics

Xing Lu, Yuxin Deng, Yanli Pei, Zimin Chen, and Gang Wang†

State Key Laboratory of Optoelectronic Materials and Technologies, School of Electronics and Information Technology, Sun Yat-Sen University, Guangzhou 510275, China

Abstract: Beta gallium oxide (β-Ga_2O_3) has attracted significant attention for applications in power electronics due to its ultra-wide bandgap of ~ 4.8 eV and the large critical electric field of 8 MV/cm. These properties yield a high Baliga's figures of merit (BFOM) of more than 3000. Though β-Ga_2O_3 possesses superior material properties, the lack of p-type doping is the main obstacle that hinders the development of β-Ga_2O_3-based power devices for commercial use. Constructing heterojunctions by employing other p-type materials has been proven to be a feasible solution to this issue. Nickel oxide (NiO) is the most promising candidate due to its wide band gap of 3.6–4.0 eV. So far, remarkable progress has been made in NiO/β-Ga_2O_3 heterojunction power devices. This review aims to summarize recent advances in the construction, characterization, and device performance of the NiO/β-Ga_2O_3 heterojunction power devices. The crystallinity, band structure, and carrier transport property of the sputtered NiO/β-Ga_2O_3 heterojunctions are discussed. Various device architectures, including the NiO/β-Ga_2O_3 heterojunction pn diodes (HJDs), junction barrier Schottky (JBS) diodes, and junction field effect transistors (JFET), as well as the edge terminations and super-junctions based on the NiO/β-Ga_2O_3 heterojunction, are described.

Key words: gallium oxide (Ga_2O_3); nickel oxide (NiO); heterojunction; power devices

Citation: X Lu, Y X Deng, Y L Pei, Z M Chen, and G Wang, Recent advances in NiO/Ga_2O_3 heterojunctions for power electronics[J]. *J. Semicond.*, 2023, 44(6), 061802. https://doi.org/10.1088/1674-4926/44/6/061802

---

1. Introduction

Power devices have been widely used in switch control and high-power circuit driving, which play an essential role in multiple applications. With the fast development of electric automobiles, fifth-generation (5G) networks, and the internet of things (IoT), silicon material has generally reached its physical limit, and traditional silicon-based power electronics have been hard to satisfy the demand for many ultra-high power applications. Wide bandgap semiconductor materials such as silicon carbide (SiC), gallium nitride (GaN), diamond, and gallium oxide (Ga_2O_3) possess attractive properties and are considered potential candidates for next-generation power devices[1, 2]. Among these, Ga_2O_3 has attracted significant attention due to its large critical electric field of 8 MV/cm and the high Baliga's figure of merit (BFOM) of more than 3000[3–5]. The BFOM of Ga_2O_3 is much higher than that of Si, SiC, and GaN, indicating that Ga_2O_3-based devices can achieve higher breakdown voltage (BV) and lower specific on-resistance ($R_{on,sp}$) simultaneously. Table 1 compares the critical material parameters of several competing power electronics semiconductors. There are five phases of Ga_2O_3 labeled as α, β, γ, δ and ε. The monoclinic β-Ga_2O_3 is the most stable[6] and is commonly studied in fabricating power devices. Large-size β-Ga_2O_3 bulk substrates can be synthesized by the low-coat melt-growth methods, such as floating zone (FZ) and edge-defined film-fed growth (EFG)[7, 8], providing significant benefits for future mass production of electronic devices. Furthermore, high-quality homoepitaxy of β-Ga_2O_3 thin films can be realized by halide vapor phase epitaxy (HVPE), metal-organic chemical vapor deposition (MOCVD), and molecular beam epitaxy (MBE)[9–14].

N-type conduction in β-Ga_2O_3 with a tunable doping concentration ranging from 10^{15} to 10^{19} cm^{-3} has been demonstrated by Si and Sn doping[8, 15, 16]. However, due to the large activation energy of acceptors and the large self-trapping energy of holes[17, 18], p-type conduction in β-Ga_2O_3 is proven difficult. The absence of p-type β-Ga_2O_3 is a major obstacle limiting the design of β-Ga_2O_3-based bipolar devices. A bipolar structure usually possesses low leakage current, high thermal stability, and good surge handling capability, which is much preferred over the unipolar configuration for power electronics. However, due to the lack of p-type doping, the studies of β-Ga_2O_3 power devices are mainly focused on unipolar devices such as Schottky barrier diodes (SBDs) and metal–oxide–semiconductor field effect transistors (MOSFETs)[19–22]. To overcome the obstacle, one possible solution is employing other p-type semiconductors and forming heterojunctions with β-Ga_2O_3. Abundant investigations have been demonstrated on β-Ga_2O_3 heterojunctions using various p-type semiconductors such as SiC, GaN, SnO, Cu_2O, CuI, and NiO[23–30]. Among these, NiO is considered the most promising choice owing to its wide bandgap of 3.6-4.0 eV and controllable p-type doping with decent mobility[25–27, 31]. Very recently, the first kilovolt-class NiO/β-Ga_2O_3 heterojunction pn diodes (HJDs) were successfully demonstrated by sputtering a p-NiO layer on β-Ga_2O_3, which opened up a route toward future bipolar operation of β-Ga_2O_3 power electronics[27]. Following that, remarkable progress has been made by many researchers in improving the BFOM of the

---

Correspondence to: G Wang, stswangg@mail.sysu.edu.cn
Received 27 DECEMBER 2022; Revised 24 FEBRUARY 2023.

Table 1. Material properties of Ga_2O_3 and some competing semiconductors for power electronics.

Material	Si	GaAs	4H-SiC	GaN	Diamond	Ga_2O_3
Band gap (eV)	1.1	1.43	3.25	3.4	5.5	4.6–4.9
Critical electric field (MV/cm)	0.3	0.4	2.5	3.3	10	8
Electron mobility (cm^2/(V·s))	1480	8400	1000	1250	2000	300
Dielectric constant	11.8	12.9	9.7	9	5.5	10
Baliga FOM ($\varepsilon\mu E_c^3$)	1	14.7	317	846	24660	>3000

NiO/β-Ga_2O_3 HJDs. Furthermore, the NiO/β-Ga_2O_3 heterojunction has been adopted into other device architectures such as junction barrier Schottky diodes (JBSs)[32], junction field effect transistors (JFETs)[33] and edge termination structures[34, 35].

This paper presents a detailed overview of the recent progress in NiO/β-Ga_2O_3 heterojunction power devices. Section 2 discusses the construction and characterization of the sputtered NiO/β-Ga_2O_3 heterojunction, focusing on its crystallinity, band structure, and carrier transport property. Section 3 and section 4 deal with the device technologies, including the NiO/β-Ga_2O_3 HJDs, JBSs, and JFETs, as well as the edge terminations and super-junctions based on the NiO/β-Ga_2O_3 heterojunction.

2. Construction and characterization of NiO/β-Ga_2O_3 heterojunction

2.1. Construction of high-voltage NiO/β-Ga_2O_3 heterojunction

NiO thin films can be grown by several techniques such as sol-gel spin coating, radio frequency (RF) sputtering, pulsed laser deposition (PLD), atomic layer deposition (ALD), MBE, and thermal oxidation of Ni[31, 36–42]. The initial study of NiO/β-Ga_2O_3 heterojunction was reported by Kokubun *et al.* in 2016[26]. A Li-doped NiO layer was grown on a 0.4-mm-thick (100) β-Ga_2O_3 single-crystal substrate ($n = 5 \times 10^{17}$ cm^{-3}) by the sol-gel spin coating technique. The device schematic and current–voltage (I–V) characteristics of the sol-gel NiO/β-Ga_2O_3 HJD are shown in Fig. 1. The device exhibited a high rectifying ratio of over 10^8 at ±3 V. However, the large $R_{\text{on,sp}}$ of approximate 1 Ω·cm^2 and low BV of 46 V indicated a suboptimal device performance for power applications. Tadjer *et al.*[41] reported the construction of NiO/β-Ga_2O_3 HJDs using sputtered and ALD-deposited NiO thin films. However, the fabricated devices showed either a very low forward current or a high reverse leakage current, which failed to satisfy the demand for power electronics. The NiO/β-Ga_2O_3 heterojunctions have also been fabricated by PLD for UV detection applications[43–46], yet the problem of high reverse current still existed.

In 2020, the first kilovolt-class NiO/β-Ga_2O_3 HJD was successfully demonstrated by sputtering a p-NiO thin film onto an epitaxial n$^-$-β-Ga_2O_3 drift layer[27], as shown in Fig. 2. The NiO films were sputtered from a NiO target at room temperature and 3 mTorr pressure in a mixture of Ar/O_2 ambient with RF power of 150 W. According to the Hall measurement, the hole concentration and hall mobility of the NiO were 1×10^{19} cm^{-3} and 0.24 cm^2/(V·s), respectively. The fabricated NiO/β-Ga_2O_3 HJDs featured a high BV of over 1 kV with an ultra-low leakage current of below 1 μA/cm^2, representing a key milestone for the development of NiO/β-Ga_2O_3 heterojunction-based power devices. So far, RF sputtering has become the optimal method for depositing NiO on β-Ga_2O_3, and continuous breakthrough has been achieved in the NiO/β-Ga_2O_3 heterojunction-based power devices.

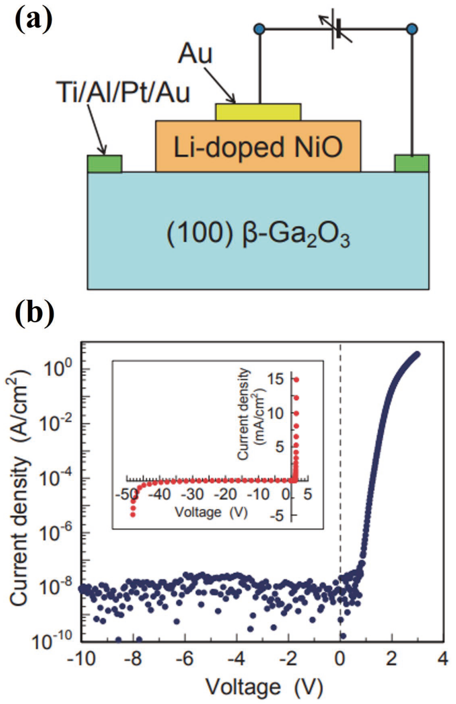

Fig. 1. (Color online) (a) Device schematic and (b) I–V characteristics of the sol-gel NiO/β-Ga_2O_3 heterojunction diode. Reproduced from Ref. [26]. Copyright 2016, The Japan Society of Applied Physics.

2.2. Crystallinity and band structure of sputtered NiO/β-Ga_2O_3 heterojunction

X-ray diffraction (XRD) measurements and high-resolution transmission electron microscopy (HRTEM) observations have been used to investigate the crystallinity of the sputtered NiO/β-Ga_2O_3 heterojunction. Several reports have identified that the sputtered NiO films were polycrystalline even after a post-deposition annealing (PDA) process[25, 27, 47–49]. As shown in Fig. 3(a), three diffraction peaks located at around 37.3°, 43.2° and 63.1° could be observed in the XRD patterns of the sputtered NiO films, which corresponded to the (111), (200), and (220) planes of NiO, respectively[48]. The HRTEM image in Fig. 3(b) also revealed that the sputtered NiO film was generally polycrystalline with fine nanocrystalline grains and a seamless contact was formed at the NiO/β-Ga_2O_3 heterojunction interface. By comparing the XRD patterns and HRTEM images of the NiO films sputtered on ($\bar{2}$01), (001), and (010) oriented β-Ga_2O_3 substrates, a very recent study pointed out that the crystallinity of sputtered NiO showed no

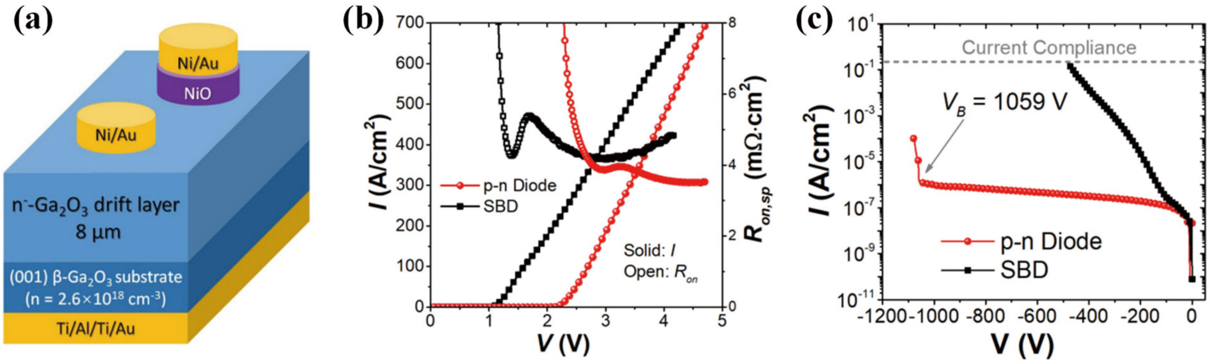

Fig. 2. (Color online) (a) Schematic of the first kilovolt-class NiO/β-Ga_2O_3 heterojunction diode. The (b) forward and (c) reverse *I*–*V* characteristics of the devices. Reproduced from Ref. [27]. Copyright 2020, IEEE.

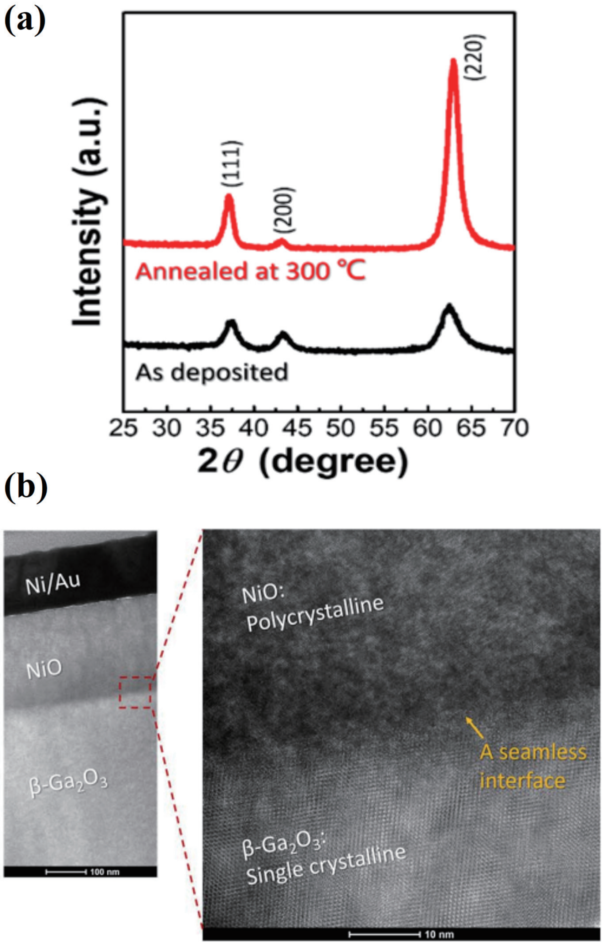

Fig. 3. (Color online) (a) XRD patterns of the sputtered NiO film on sapphire before and after annealing. (b) Cross-sectional HRTEM images of the NiO/β-Ga_2O_3 heterojunction interface. Reproduced from Ref. [48]. Copyright 2021, IEEE.

strong dependency on the β-Ga_2O_3 substrate orientations[47].

It is known that the band structure of a heterojunction is crucial for device design and application. The band alignment of the heterojunction greatly influences its carrier transport properties. Thus it is essential to characterize the band offset at the heterojunction interface accurately. Gong *et al.*[50] reported a type-II band alignment of the sputtered NiO/β-Ga_2O_3 heterojunction with a valence band offset (VBO) of 3.60 eV and conduction band offset (CBO) of 2.68 eV. In comparison, Zhang *et al.*[45] reported a VBO value of 2.1 eV and CBO value of 0.9 eV for a similar sputtered NiO/β-Ga_2O_3 heterojunction. The band alignment of the sputtered NiO/β-Ga_2O_3 heterojunctions varies from each other, which could be determined by many factors, such as the strain, defects/vacancies, interfacial contamination, crystal orientation, and so on. Due to the crystalline anisotropy, β-Ga_2O_3 possesses anisotropic material properties and devices with different orientations show different performances[14, 51–56]. The substrate orientation-dependent band alignment of the NiO/β-Ga_2O_3 heterojunctions was investigated by an X-ray photoelectron spectroscopy (XPS) analysis[47]. The VBO values of the NiO/β-Ga_2O_3 heterojunctions were extracted to be 2.12 ± 0.06, 2.44 ± 0.07, and 2.66 ± 0.07 eV for ($\bar{2}$01), (001) and (010) β-Ga_2O_3 substrates, respectively. The determined energy band diagrams of the NiO/β-Ga_2O_3 heterojunctions with different β-Ga_2O_3 orientations are shown in Fig. 4. The influence of a PDA process on the band alignment of the NiO/β-Ga_2O_3 heterojunction was studied by Xia *et al.*[57]. As shown in Fig. 5, the band offsets monotonically increased while the bandgap of NiO decreased with the elevated annealing temperature up to 600 °C. The results also indicated a possible unstable performance of the NiO/β-Ga_2O_3 heterojunction device at high temperatures.

2.3. Carrier transport mechanisms in the sputtered NiO/β-Ga_2O_3 heterojunction

Several groups have identified different forward conduction mechanisms rather than the conventional diffusion theory in the NiO/β-Ga_2O_3 heterojunction[48, 50, 58]. Due to the high barrier height against carriers in the type-II band structure, the diffusion and emission currents in the NiO/β-Ga_2O_3 heterojunction are negligible at a low forward bias. When the low forward bias is below 1.6 V, interface recombination has been revealed to be the dominant forward conduction mechanism of the NiO/β-Ga_2O_3 heterojunctions[48, 50], in which the electrons and holes recombined once they meet at the heterojunction interface by overcoming the barrier of the depletion region. For an asymmetric heterojunction, the interface recombination current can be expressed as the following equation according to Grundmann *et al.*[59]

$$J_{\rm reco}(V)=\zeta\frac{qV}{kT}\sqrt{\frac{2kT}{\varepsilon_{\rm s}}\sigma_{\rm n}\sigma_{\rm p}n_0}\exp\left(\frac{-qV_{\rm bi}}{2kT}\right)\exp\left(\frac{qV}{2kT}\right),$$

where k and T are the Boltzmann's constant and the temperature, $\varepsilon_{\rm s}$ and n_0 are the dielectric constant and electron concentration of the β-Ga_2O_3, $V_{\rm bi}$ is the build-in potential in the

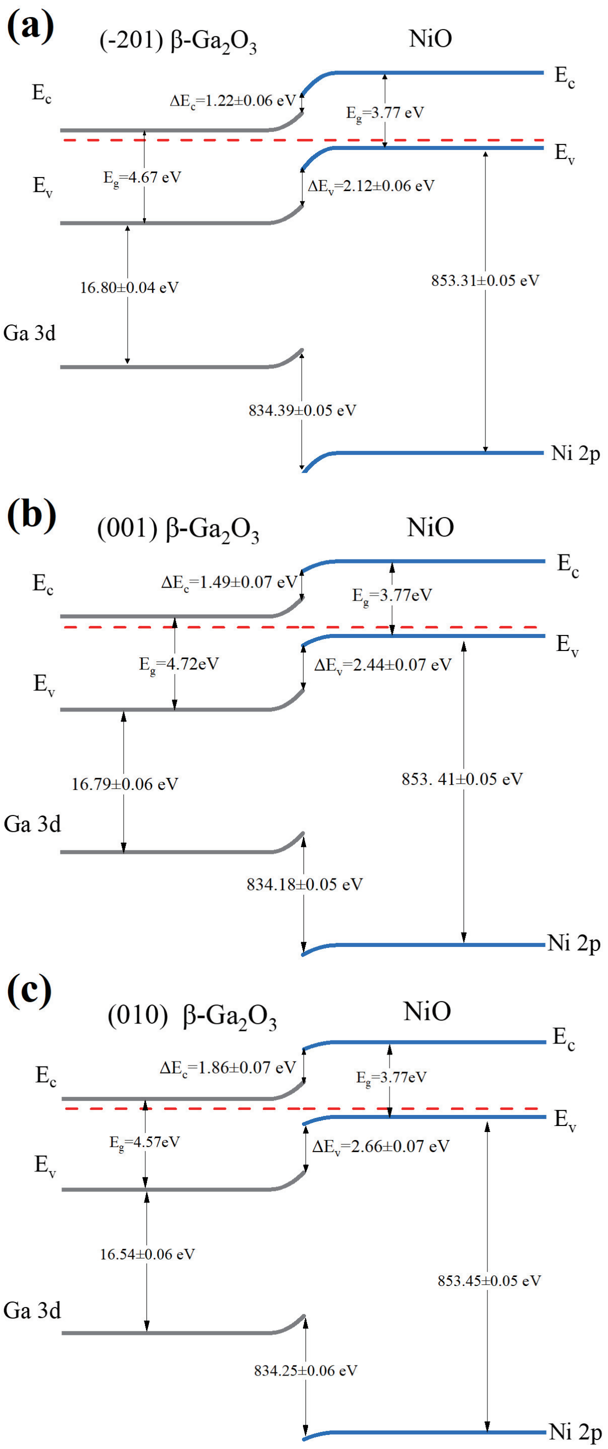

Fig. 4. (Color online) The energy band diagrams of the NiO/β-Ga$_2$O$_3$ heterojunctions at thermal equilibrium with different β-Ga$_2$O$_3$ substrate orientations. Reproduced from Ref. [47]. Copyright 2023, Elsevier B.V.

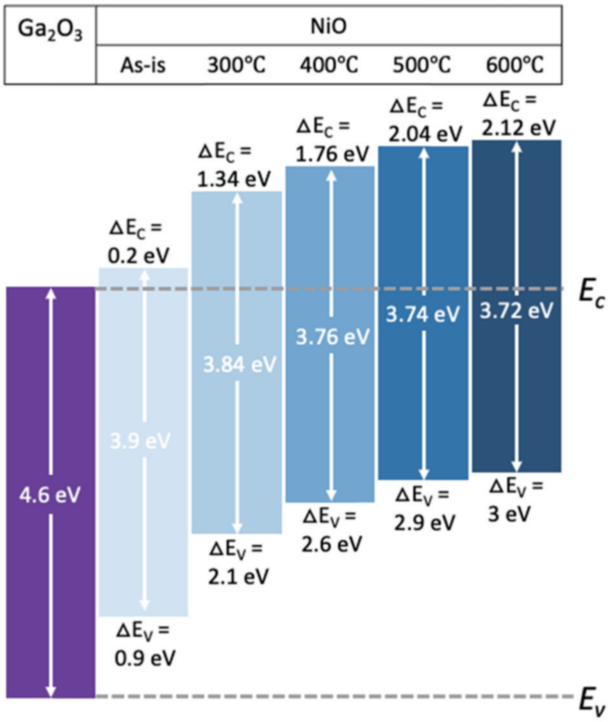

Fig. 5. (Color online) Band alignments of the NiO/β-Ga$_2$O$_3$ heterojunctions as a function of post-deposition annealing temperature. Reproduced from Ref. [57]. Copyright 2022, IOP Publishing Ltd.

NiO/β-Ga$_2$O$_3$ heterojunction, and σ_n and σ_p are the conductivities of β-Ga$_2$O$_3$ and NiO, respectively. The coefficient $\zeta = 1$ or $\zeta \to 0$ represents the fast or low recombination occurring at the heterojunction interface. A near-zero ζ of ~0.008 was obtained for the sputtered NiO/β-Ga$_2$O$_3$ heterojunction at room temperature, indicating a relatively slow recombination. Given $V_{\rm bi}$ = 1.9 V from *C*–*V* measurement, Gong *et al.*[50] also revealed a small ζ which decreased from 5.4×10^{-4} to 3.4×10^{-6} when the applied bias varied from $V_{\rm bi}/2$ to $V_{\rm bi}$. Due to the large VBO (> 2 eV) of the NiO/β-Ga$_2$O$_3$ heterojunction, the holes in NiO can hardly be injected across the barrier at a low forward bias. Instead, the electrons contributed by β-Ga$_2$O$_3$ recombine with the holes in the valence band of NiO through interfacial states, which forms the interface recombination current.

When the forward bias increased (>1.6 V), a trap-assisted multistep tunneling model became the dominant conduction mechanism in the NiO/β-Ga$_2$O$_3$ heterojunction[48]. The model can be described by the following equation[60, 61]

$$J_{\rm tunnel}\,(V) = J_{\rm t0}\exp\left(\alpha\theta^{\frac{1}{2}}V\right),$$

$$J_{\rm t0} = BN_{\rm T}\exp\left(-\alpha\theta^{\frac{1}{2}}V_{\rm bi}\right),$$

where $\alpha = (4/3\hbar)\sqrt{m^*\varepsilon_{\rm s}/N_{\rm D}}$, $N_{\rm D}$ is the doping concentration of β-Ga$_2$O$_3$, θ is the number of steps of the tunneling, and B is a constant. Fig. 6(a) shows the fitting result of the two models, as mentioned above, with the experimental forward *I*–*V* characteristics of the NiO/β-Ga$_2$O$_3$ heterojunction diodes at different temperatures, which exhibits a good agreement. The extracted $\ln(J_{\rm t0})$ as a function of temperature showing good linearity further confirmed the multistep tunneling mechanism, as shown in Fig. 6(b). It is speculated that the grain boundaries in the sputtered NiO films act as trap states[48] and facilitate electron tunneling[62]. In addition, according to the deep-level transient spectroscopy (DLTS) measurements carried out at a fixed reverse voltage of –6 V, a pulse filling voltage of +1 V, a pulse filling time of 0.02 ms, and a frequency of 1 Hz[63], an electron trap corresponded to the forward trap-assisted tunneling was observed in the spectra for the NiO/β-Ga$_2$O$_3$ heterojunction. This electron trap ($E_{\rm T}$) exhibited an energy level of $E_{\rm C}$ – 0.67 eV, which is related to Fe sub-

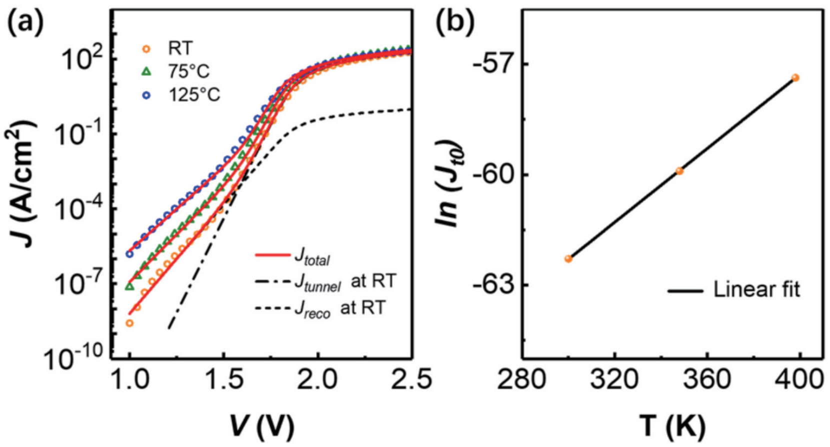

Fig. 6. (Color online) (a) Temperature-dependent forward $I-V$ characteristics and the fitting result with the interface recombination and trap-assisted tunneling current model. (b) ln(J_{t0}) versus temperature plot for the NiO/β-Ga_2O_3 heterojunction. Reproduced from Ref. [48]. Copyright 2021, IEEE.

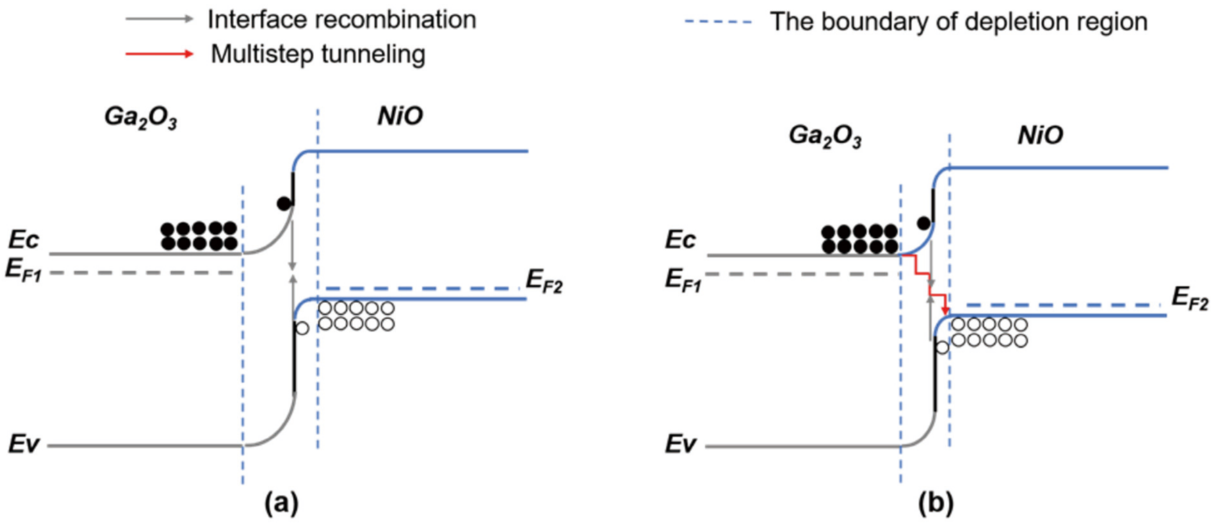

Fig. 7. (Color online) Energy band diagrams of the NiO/β-Ga_2O_3 heterojunction p−n diode at a (a) low and (b) high forward bias. Reproduced from Ref. [48]. Copyright 2021, IEEE.

stituting for Ga on a tetrahedral site (Fe_{GaI})[64]. It has been confirmed that Fe impurities unintentionally doped in the EFG bulk β-Ga_2O_3 during the crystal growth[65], which might be the possible origination of the E_T. Fig. 7 shows the energy band diagrams and carrier dynamics of the NiO/β-Ga_2O_3 heterojunction.

When the forward bias went beyond 3.5 V, a high-level injection phenomenon and corresponding conductivity modulation effect were observed[62]. This is because the energy band of NiO is pulled down at a very high forward bias, which leads to a significantly reduced hole barrier height at the Fermi tail; thus, the holes in NiO can travel across the heterojunction interface and diffuse into β-Ga_2O_3. DLTS spectra performed at the same condition in Ref. [63] but with frequency of 1200 Hz exhibited two positive peaks, which are the distinctive contribution by hole traps (H_T). The detection of H_T further confirmed the hole injection from p-NiO to β-Ga_2O_3 in the heterojunction.

3. Device technology based on the NiO/β-Ga_2O_3 heterojunction

Possessing the advantages of low leakage current, high thermal stability, and good surge handling capability, bipolar power devices based on pn junctions have always attracted great attention, which promotes the blossoming of the NiO/β-Ga_2O_3 heterojunction-based power electronics. Very recently, a high BFOM of 13.21 GW/cm² was successfully demonstrated in an 8-kV class sputtered NiO/β-Ga_2O_3 HJD, representing the highest BFOM value among all the reported β-Ga_2O_3 power devices[62]. Besides, high-performance JBSs[32] and JFETs[33] based on the NiO/β-Ga_2O_3 heterojunctions have been developed by several groups. Implementation of the NiO/β-Ga_2O_3 heterojunctions as edge terminations and super-junctions in various types of β-Ga_2O_3 power devices has been promised[34, 35]. Fig. 8 lists some milestones in developing state-of-the-art NiO/β-Ga_2O_3 heterojunction based power devices.

3.1. NiO/β-Ga_2O_3 heterojunction diodes

As previously mentioned, the first 1 kV NiO/β-Ga_2O_3 HJDs[27] were fabricated using an 8-μm thick lightly doped (n = 4 × 10^{16} cm^{-3}) β-Ga_2O_3 drift layer grown on a conductive (n = 2.6 × 10^{18} cm^{-3}) (001) substrate with a 200-nm thick sputtered p-NiO layer (p = 1 × 10^{19} cm^{-3}) on top. The device yielded a BV of 1059 V with an ultra-low leakage current of

X Lu et al.: Recent advances in NiO/Ga₂O₃ heterojunctions for power electronics

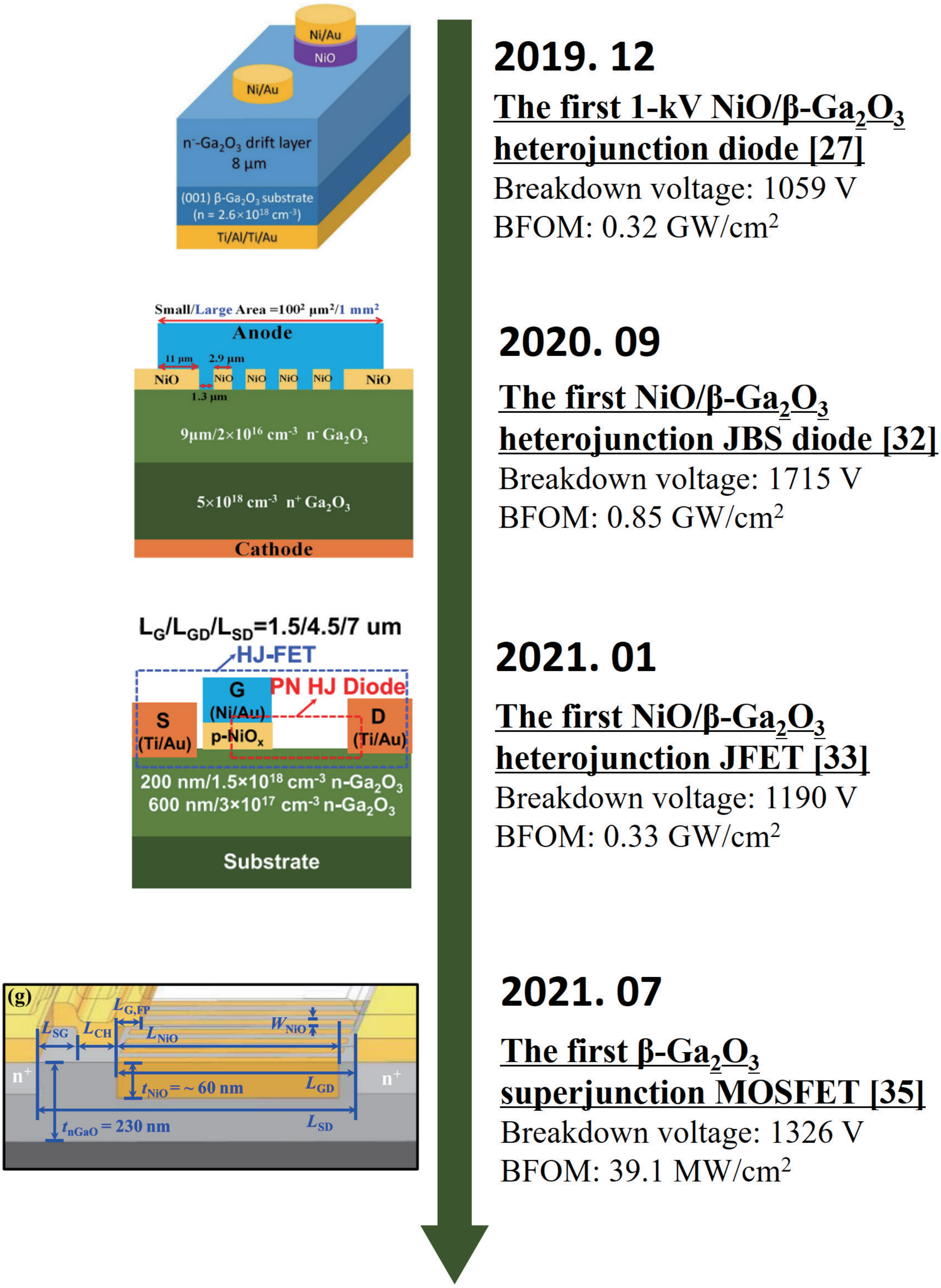

Fig. 8. (Color online) The milestones of the state-of-the-art NiO/β-Ga$_2$O$_3$ heterojunction based power devices. Reproduced from Refs. [27, 32, 33, 35]. Copyright 2021 and 2022, IEEE.

below 10^{-6} A/cm^2 before breakdown and a low $R_{\text{on,sp}}$ of 3.5 mΩ·cm^2, leading to a BFOM of 0.32 GW/cm^2. The results pave the way for developing high-performance bipolar power devices based on the NiO/β-Ga$_2$O$_3$ heterojunctions.

The trap states located within the sputtered NiO and at the heterojunction interface significantly affect the device performance of a NiO/β-Ga$_2$O$_3$ HJD. A PDA process has been proven as an effective method to improve the crystallinity of the sputtered NiO and reduce the defects density at the hetero-interface[48, 49, 66]. Moreover, the PDA process could also improve the metal-to-NiO Ohmic contact. Through a precisely controlled PDA process, Hao *et al.*[66] demonstrated the performance improved NiO/β-Ga$_2$O$_3$ HJDs. After annealing at 350 °C for 3 min in a nitrogen atmosphere, the $R_{\text{on,sp}}$ of the HJD was reduced from 5.4 to 4.1 mΩ·cm^2 while the BV increased from 900 to 1630 V, leading to an improved BFOM from 0.16 to 0.65 GW/cm^2 as shown in Fig. 9. The ideality factor was extracted to be 3.02 and 1.27 for devices without and

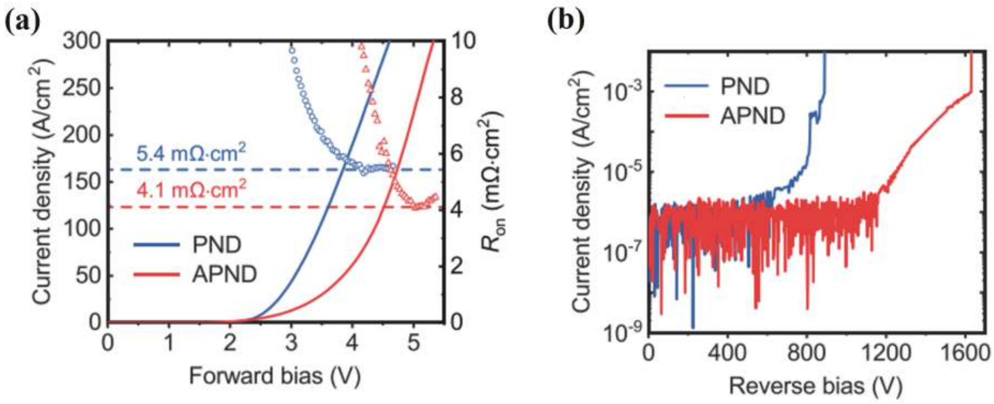

Fig. 9. (Color online) The (a) forward and (b) reverse *I*–*V* characteristics of the NiO/β-Ga_2O_3 heterojunction diodes with and without annealing. Reproduced from Ref. [66]. Copyright 2021, AIP Publishing.

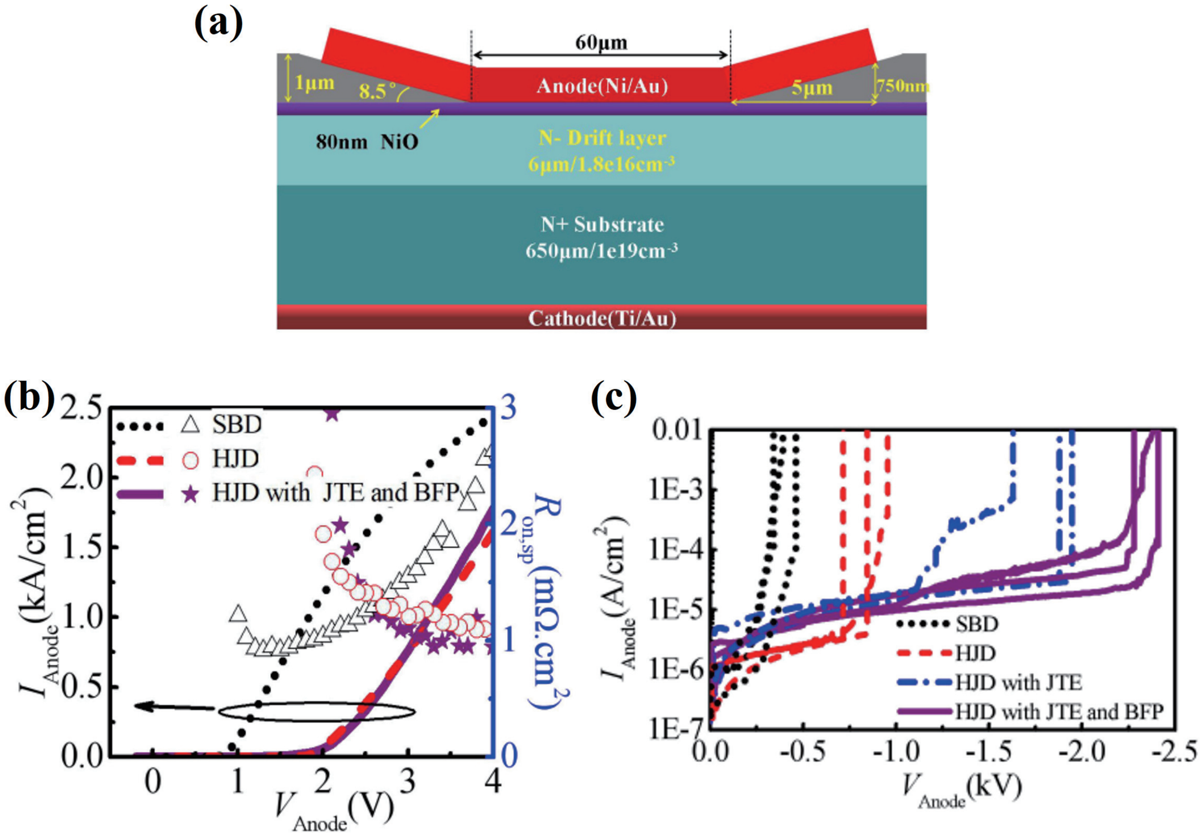

Fig. 10. (Color online) (a) Cross-sectional schematic of the NiO/β-Ga_2O_3 heterojunction with small-angle bevel FP. The (b) forward and (c) reverse *I*–*V* characteristics of the devices. Reproduced from Ref. [25]. Copyright 2022, IEEE.

with annealing, and the calculated interface trap density (N_t) were about 1.04×10^{12} and 1.33×10^{11} eV^{-1}, respectively.

Various field plate (FP) structures have been implemented in the NiO/β-Ga_2O_3 HJDs to manage the electric field. Gong *et al.*[67] reported a double-layered insulating FP structure. The first layer insulator was a 350-nm-thick SiN_x layer deposited by plasma enhanced chemical vapor deposition (PECVD) at 300 °C and the second layer insulator was a 40-nm-thick Al_2O_3 layer grown by ALD at 300 °C. Subsequently, a 300 nm NiO layer with a length of field plate (L_{FP}) of 10 μm was deposited by RF sputtering. A PDA process was carried out at 300 °C in air for 1 h. The device demonstrated a BV of 1036 V and a $R_{on,sp}$ of 5.4 mΩ·cm². A small-angle bevel FP structure was proposed for the NiO/β-Ga_2O_3 HJDs by Wang *et al.*[25], as shown in Fig. 10. To realize the small-angel bevel FP, a 1-μm thick SiO_2 was deposited by PECVD and dry etched using a photoresist mask formed by a variable-temperature photoresist reflow technique. The device featured a BV of up to 2410 V with a low $R_{on,sp}$ of 1.12 mΩ·cm², yielding a high BFOM of 5.18 GW/cm². The bevel angle of the FP, the dielectric layer thickness, and the dimension of the FP are the critical parameters. With well-optimized parameters, this FP structure can offer great potential for fabricating high-voltage β-Ga_2O_3 power devices.

Another approach to improve the performance of the NiO/β-Ga_2O_3 HJDs is using a double-layered NiO film[68]. As shown in Fig. 11(a), the sputtered NiO film was composed of a 350-nm-thick lower-side lightly doped layer (p = 5.1×10^{17} cm^{-3}) and a 100-nm-thick upper-side heavily doped layer (p = 3.6×10^{19} cm^{-3}). Compared with the single-layered

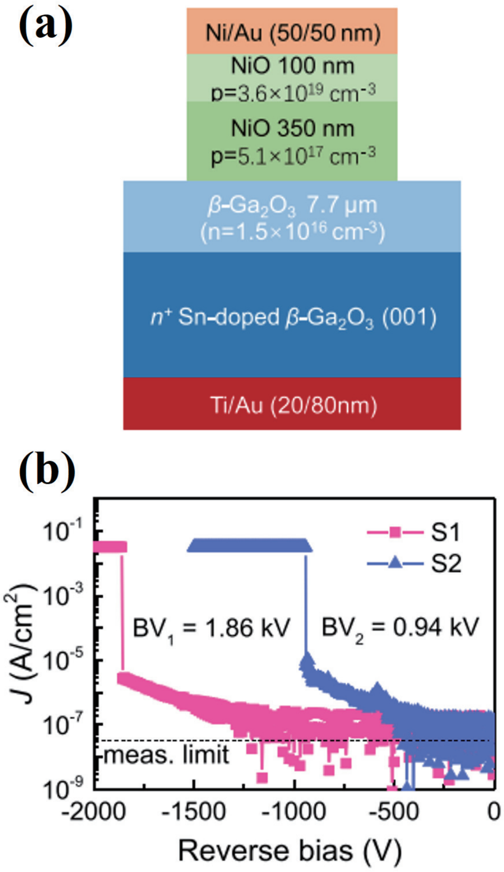

Fig. 11. (Color online) (a) Device schematic and (b) the reverse *I*–*V* characteristics of the double-layered NiO/β-Ga_2O_3 heterojunction diode. Reproduced from Ref. [68]. Copyright 2020, AIP Publishing.

device (S2), the double-layered device (S1) demonstrated an enhanced BV from 0.94 to 1.86 kV, as shown in Fig. 11(b). Liao *et al.*[49] thoroughly optimized the double-layered NiO/β-Ga_2O_3 HJDs by performing both experimental study and technology computer-aided design (TCAD) simulation. It was revealed that the bottom lightly doped NiO layer could smoothen the electric field, while the upper heavily doped NiO layer can reduce the $R_{on,sp}$ by lowering the metal-to-NiO contact resistance. In addition, verified by the TCAD simulation, the electric field peak of the double-layered NiO/β-Ga_2O_3 HJDs located at the edge of the p^+-NiO layer rather than the p^--NiO layer, and enlarging the dimension of the bottom p^--NiO layer can effectively suppress the electric field peak, as shown in Fig. 12. The influence of the bottom NiO layer thickness was studied by Li *et al*.[69]. The device schematic is shown in Fig. 13(a). The upper NiO layer (p = 2.6 × 10^{19} cm^{-3}) was fixed at 10 nm, while the thickness of the bottom NiO layer (p = 3 × 10^{18} cm^{-3}) ranged from 10 nm to 80 nm. The BV showed a negative correlation with the thickness of the bottom NiO layer, as shown in Fig. 13(b).

Zhou *et al.*[70] demonstrated a novel beveled-mesa NiO/β-Ga_2O_3 HJD, as shown in Fig. 14. By precisely adjusting the gap between the mask and β-Ga_2O_3 wafer as well as the declination angle of the NiO target with respect to the substrate surface normal, the double-layered NiO film with a small beveled angle was formed. The fabricated large-area (1 mm^2) HJDs performed a low $R_{on,sp}$ of 2.26 mΩ·cm^2 and a high BV of 2.04 kV, leading to a BFOM of 1.84 GW/cm^2. A remarkable BV of 8.32 kV was achieved in the NiO/β-Ga_2O_3 HJD[62] by employing the double-layered NiO structure and advanced edge terminations of an FP and an Mg-implanted guard ring. Ion implantation in the device periphery to form a high-resistivity region can effectively relieve the electric field crowing effect and improve the breakdown voltage in power devices. Fig. 15 shows the schematic and *I*–*V* characteristics of the device. A low $R_{on,sp}$ of 5.24 mΩ·cm^2 was obtained for the 8.32 kV HJD, and the BFOM of 13.21 GW/cm^2 was the highest value among all the reported β-Ga_2O_3 power devices so far.

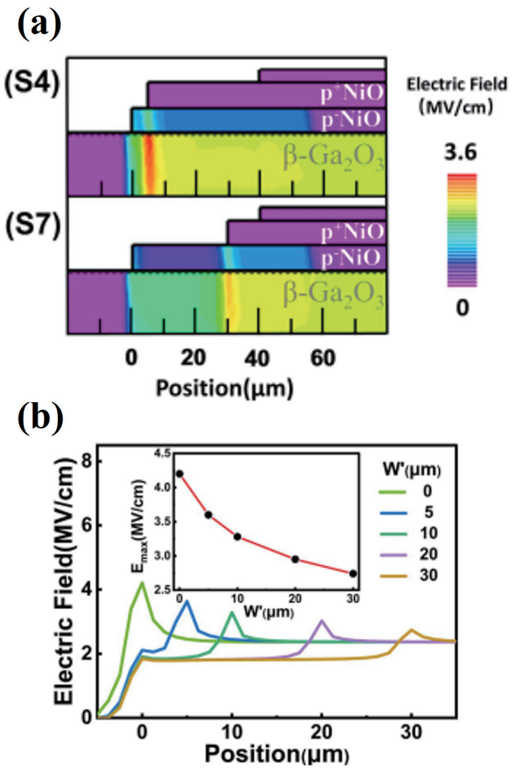

Fig. 12. (Color online) (a) Simulated two-dimensional electric field distributions in the vicinity of the NiO and anode electrode at a reverse bias of 1000 V for the double-layered NiO/β-Ga_2O_3 HJD and (b) line profile of simulated electric field along the surface of the β-Ga_2O_3 drift layer for the HJD with varied W' (W' = $R_{p\text{-}NiO}$ − R_{p+NiO}). Reproduced from Ref. [49]. Copyright 2022, IEEE.

3.2. NiO/β-Ga_2O_3 heterojunction JBS

Schottky barrier diodes (SBDs) possess properties of low turn-on voltage and fast switching speed. Meanwhile, p–n diodes have the advantages of low leakage current and good surge handling capability. The JBS devices can combine the advantages of SBDs and p–n diodes.

The first NiO/β-Ga_2O_3 heterojunction JBS was demonstrated by Lv *et al.*[32]. Fig. 16 shows the schematic and the *I*–*V* characteristics of the JBS device. The NiO layer (p = 1 × 10^{18} cm^{-3}) with a thickness of 60 nm was formed by thermally oxidizing Ni metal. The fabricated JBS showed a low V_{on} of ~1 V, slightly higher than the reference SBD (~0.7 V). The BV of the JBS was as high as 1715 V, far superior to that of the reference SBD (655 V). However, these JBSs suffered from a huge reverse leakage current under a high electric field, and the leakage mechanism was determined to be a Pool-Frenkel (PF) emission, which refers to the electric-field-

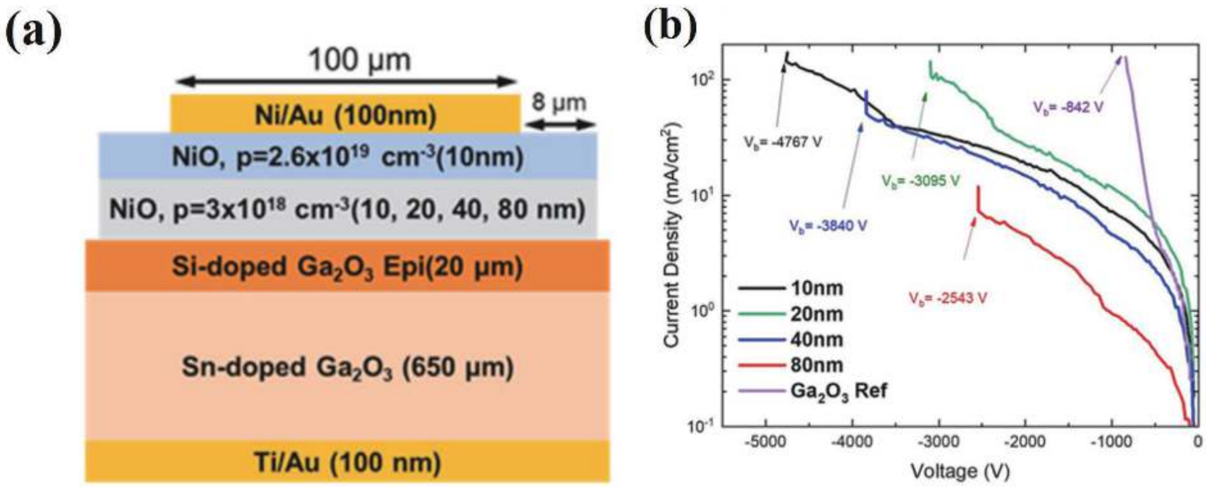

Fig. 13. (Color online) (a) Device schematic and (b) the reverse *I–V* characteristics of the double-layered NiO/β-Ga_2O_3 heterojunction diode with varied thickness of the bottom NiO layer. Reproduced from Ref. [69]. Copyright 2022, AIP Publishing.

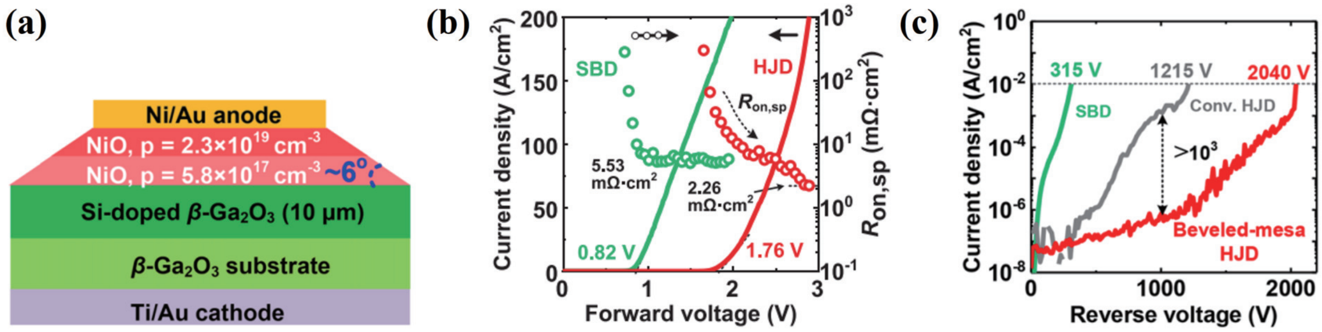

Fig. 14. (Color online) (a) Cross-sectional schematic of the NiO/β-Ga_2O_3 heterojunction diode with bevel mesa. The (b) forward and (c) reverse *I–V* characteristics of the devices. Reproduced from Ref. [70]. Copyright 2021, AIP Publishing.

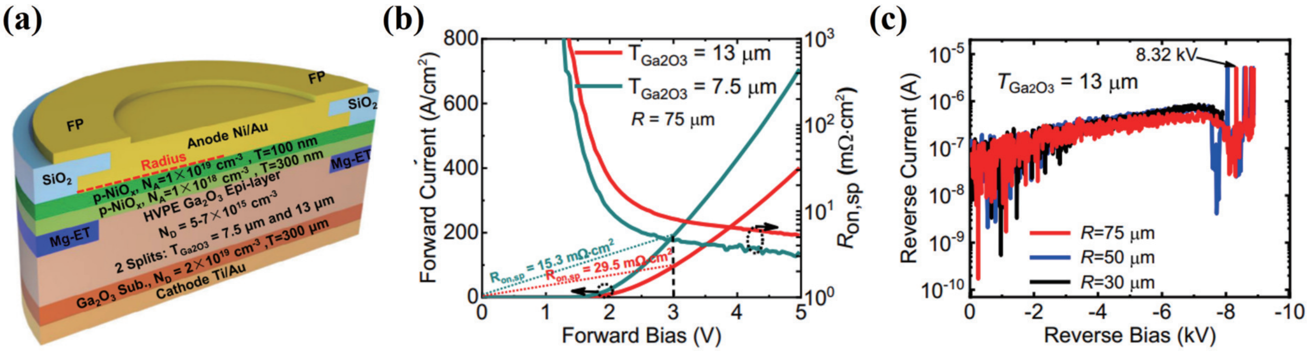

Fig. 15. (Color online) (a) Cross-sectional schematic of the NiO/β-Ga_2O_3 heterojunction diode with double NiO layer and edge termination. The (b) forward and (c) reverse *I–V* characteristics of the devices. Reproduced from Ref. [62].

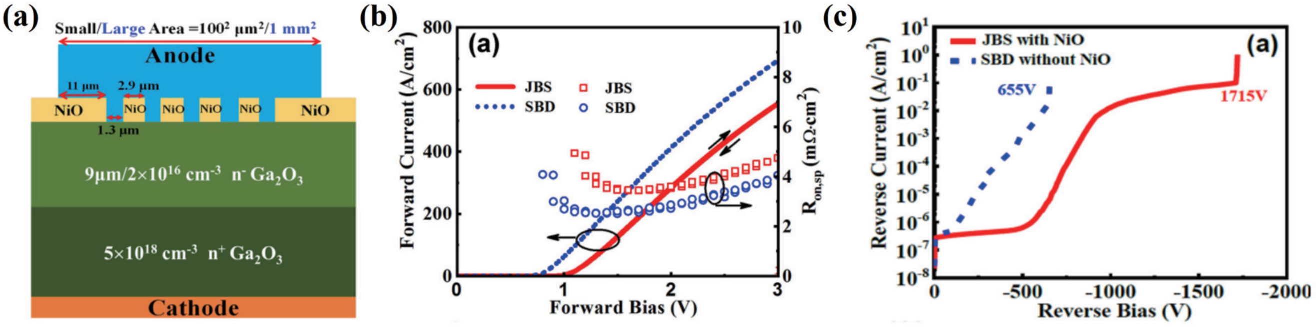

Fig. 16. (Color online) (a) Cross-sectional schematic of the NiO/β-Ga_2O_3 JBS diode. The (b) forward and (c) reverse *I –V* characteristics of the devices. Reproduced from Ref. [32]. Copyright 2021, IEEE.

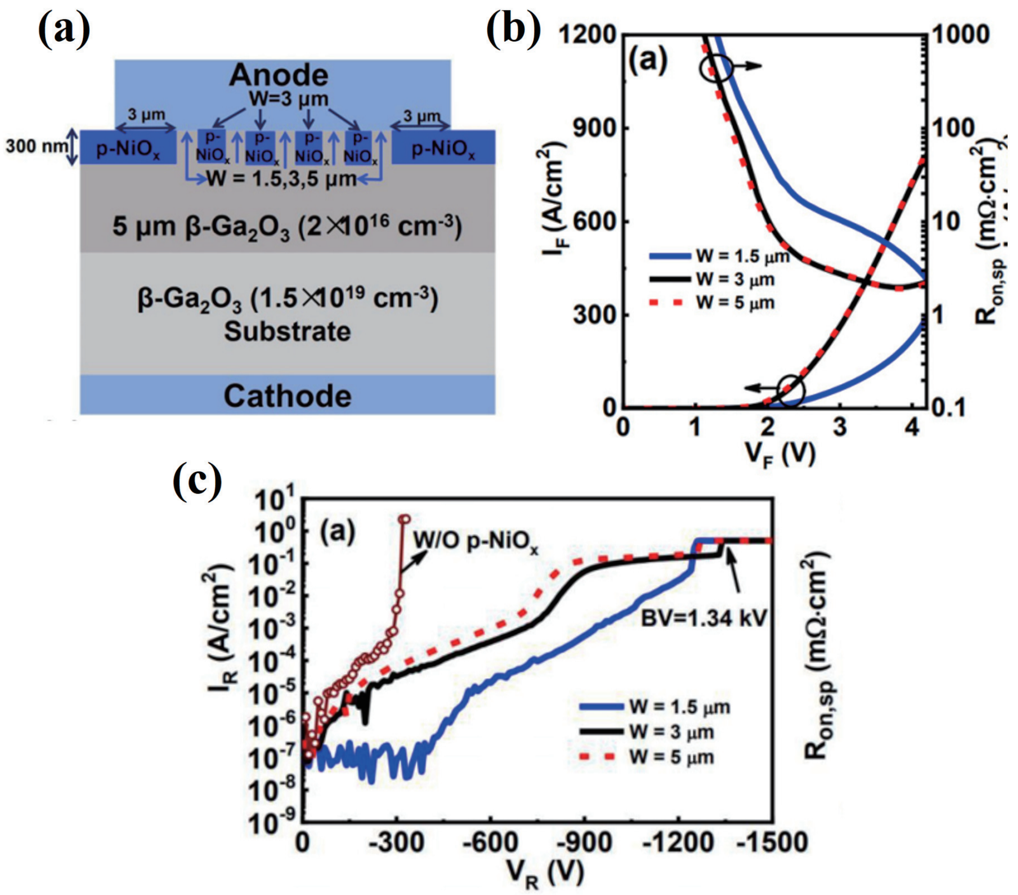

Fig. 17. (Color online) (a) Cross-sectional schematic of the NiO/β-Ga_2O_3 JBS diode with fin structure. The (b) forward and (c) reverse *I*–*V* characteristics of the devices with different fin widths. Reproduced from Ref. [73]. Copyright 2021, AIP Publishing.

enhanced thermal excitation of electrons from a trapped state into a continuum of electronic states[71]. According to the Arrhenius plots of the reverse leakage current vs. 1000/*T* measured at various reverse biases, the emission barrier height was determined to be E_C – 0.72 eV below the conduction band, which is consistent with the energy level of gallium vacancies (V_{Ga})[72]. It indicated that in such a JBS structure, the NiO/β-Ga_2O_3 heterojunction failed to suppress the reverse leakage current through the Schottky contact region. To address this issue, the NiO/β-Ga_2O_3 heterojunction JBSs with etched fin structures were developed[73]. The fin structures on the β-Ga_2O_3 drift layer were firstly formed by reactive ion etching (RIE), and then the trenches between the fins were filled with sputtered p-NiO, as schematically shown in Fig. 17(a). With the fin structures, the pn heterojunction depleted laterally at the reverse bias, which lowered the density of free carriers left in the β-Ga_2O_3 channel; thus, the fin structures would help to suppress the leakage current through the Schottky contact region. Three JBSs with different fin widths were fabricated. The V_{on} and $R_{on,sp}$ of the JBSs were measured to be 1.7 V/2.45 mΩ·cm^2, 1.5 V/1.94 mΩ·cm^2, and 1.45 V/1.91 mΩ·cm^2, for the fin width of 1.5, 3, and 5 *μ*m, respectively. Since the forward *I*–*V* characteristics of a JBS should be mainly determined by its Schottky contact region, the device had a greater proportion of Schottky contact area showed a closer value of V_{on} and $R_{on,sp}$ to an SBD. However, the measured BV of the JBSs did not show a strong dependence on the fin width. Though the reverse leakage current was partially suppressed by using the fin structures, the dry etching process produced high-density deep-level traps at the β-Ga_2O_3 surface, which might introduce excess leakage current[74, 75]. A post-etching treatment process would be helpful to remove the defects from the etched β-Ga_2O_3 surface, for example, surface treatment using a hot tetramethylammonium hydroxide (TMAH) solution[76]. At present, high reverse leakage current is still the remaining issue that hinders the development of the NiO/β-Ga_2O_3 heterojunction JBSs.

3.3. NiO/β-Ga_2O_3 heterojunction JFET

The development of lateral β-Ga_2O_3 field-effect transistors (FETs) has achieved remarkable progress[77–80]. However, the reported device performance is still far from the projected material limitation of β-Ga_2O_3. The channel doping level and thickness must be carefully designed to ensure an effective channel pinch-off in a lateral FET and obtain a good balance between the $R_{on,sp}$ and BV. The β-Ga_2O_3 JFETs based on the NiO/β-Ga_2O_3 heterojunctions have been proposed by Wang *et al.* for the first time[33], as shown in Fig. 18(a). The employed p-NiO gate provided a vertical depletion to the β-Ga_2O_3 channel and facilitated the channel pinch-off. Therefore, a relatively thicker channel and higher channel doping concentration could be used in the device to minimize the $R_{on,sp}$ without sacrificing the BV. On the other hand, the lateral depletion of the heterojunction in the channel could help smooth the electric field at the drain-side-gate-edge and boost the BV of the JFETs. The fabricated devices exhibited a low $R_{on,sp}$ of 3.19 mΩ·cm^2 and a high BV of 1115 V, yielding a BFOM of 0.39 GW/cm^2. Using a gate-recessed architecture, a

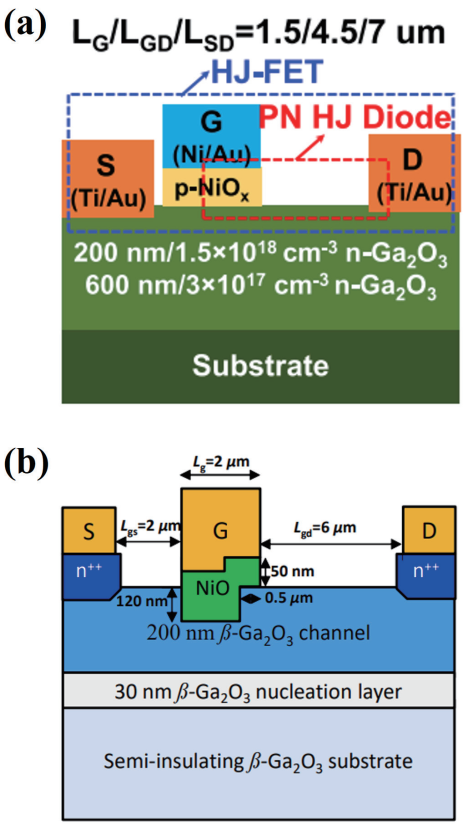

Fig. 18. (Color online) Cross-sectional schematic of (a) the NiO/β-Ga_2O_3 JFET and (b) the NiO/β-Ga_2O_3 JFET with recessed gate. Reproduced from Refs. [33, 81]. Copyright 2021 and 2022, IEEE.

normally-off operation has been realized in the NiO/β-Ga_2O_3 heterojunction JFETs[81]. As schematically shown in Fig. 18(b), the 200 nm channel was recessed down to 80 nm in the gate region by an inductively coupled plasma (ICP) etching process, and a 50 nm p-NiO gate was sputtered. A positive threshold voltage (V_{th}) of +0.9 V was achieved.

4. NiO/β-Ga_2O_3 heterojunction-based edge terminations and super-junctions

Various edge termination techniques, such as FP[19, 82], ion-implanted GR[20, 83, 84], and thermally oxidized terminations[85], have been developed to relieve the electric field crowding and enhance the BV of the β-Ga_2O_3 power device.

The field limiting ring (FLR) using p–n junctions is an effective structure to suppress the electric field peak at the device edge, which is commonly used in SiC power devices[86]. An improved BV has been reported in β-Ga_2O_3 SBDs by adopting a NiO/β-Ga_2O_3 heterojunction-based FLR[71], as shown in Fig. 19(a). Compared to the device without the FLR, the average BV was increased from 0.43 to 0.75 kV. A TCAD simulation was carried out to investigate the influence of the NiO/β-Ga_2O_3 heterojunction FLR on the electric field distribution of the devices under a reverse bias. As shown in Fig. 19(b), the electric field spread out into the FLR structures, and the crowding of the electric field at the device edge was effectively mitigated.

The p-NiO guard ring has also been employed in β-Ga_2O_3 SBDs[34]. As shown in Fig. 20, a 300-nm trench was etched in the β-Ga_2O_3 drift layer and subsequently filled with sputtered p-NiO (p = 1 × 10^{18} cm^{-3}) to construct the guard ring.

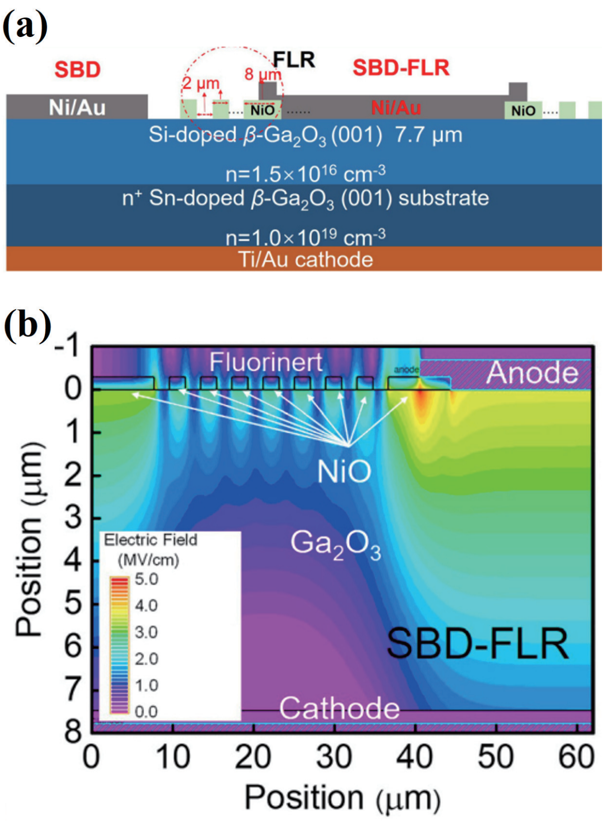

Fig. 19. (Color online) (a) Schematic of β-Ga_2O_3 SBD with FLR. (b) Two-dimensional electric field distribution at a reverse bias of 1.89 kV for β-Ga_2O_3 SBD with FLR. Reproduced from Ref. [71]. Copyright 2021, AIP Publishing.

The SBDs showed an improved BV of 1130 V by introducing the p-NiO guard ring compared to a BV of 300 V for SBDs without the guard ring. By further implementation of an FP structure, the BV was boosted to 1860 V.

Super-junction (SJ) is a promising technique to manage the electric field in power devices[87–90], which has been successfully commercialized in Si devices[91, 92] and also introduced in GaN and SiC devices[93–95]. With an alternative arrangement of p-type and n-type stripes, the SJ structure can uniform the electric field distribution in the drift layer, relying on the charge balance principle[96]. Wang *et al.*[35] demonstrated a novel super-junction β-Ga_2O_3 MOSFET based on the NiO/β-Ga_2O_3 heterojunctions, as shown in Fig. 21. Trenches in the β-Ga_2O_3 drift layer were formed using ICP etching and then filled with sputtered NiO (p = 1 × 10^{18} cm^{-3}). Compared with a co-fabricated conventional MOSFET, the SJ MOSFETs exhibited an improved BFOM by 4.86 times.

5. Summary and prospects

Still at the very early stage of development, the NiO/β-Ga_2O_3 heterojunction has shown great potential for application in β-Ga_2O_3 power electronics. In this review, we summarized the state-of-the-art device technology and development of NiO/β-Ga_2O_3 heterojunction power devices. Despite the encouraging progress, some crucial issues still exist for practical application.

First, developing high-quality β-Ga_2O_3 material, including both the substrate and the epi film, is the cornerstone for future improvement of the power devices. The unintentional

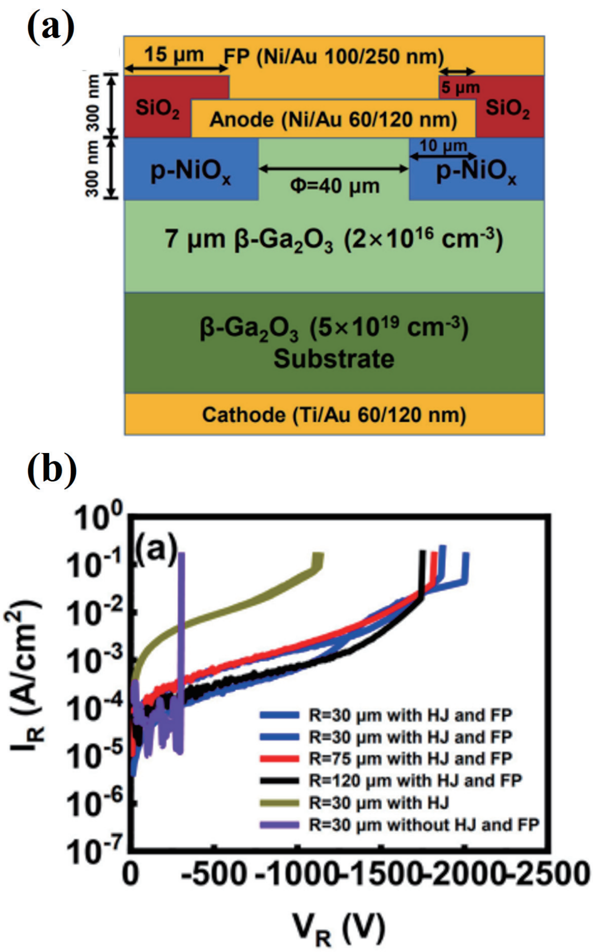

Fig. 20. (Color online) (a) Schematic of β-Ga$_2$O$_3$ SBD with NiO guard ring and FP termination. (b) Reverse *I*–*V* characteristics of β-Ga$_2$O$_3$ SBD without and with termination structure. Reproduced from Ref. [34]. Copyright 2022, AIP Publishing.

impurities, defects, and dislocations within the β-Ga$_2$O$_3$ crystal can significantly affect the device performances regarding leakage current, electrical conductivity, device reliability, etc.

The device structure optimization is essential to further enhance the device voltage blocking capability. As mentioned, the double NiO layers, FP structures, and ion-implanted GRs are all feasible solutions. Still, further improvements in the details of these structures remain. For example, the dielectric layer's materials, thickness, and deposition process are critical factors for an FP structure. As for the ion-implanted GRs, more investigation is needed on different implanted ions, the profiles of the implanted region, and the post-implantation annealing conditions.

Trap states at the NiO/β-Ga$_2$O$_3$ heterojunction interface can cause large hysteresis and excess reverse leakage current. As mentioned, a PDA process is an effective method to improve the heterojunction interface quality. However, the forward conduction can be degraded by annealing since the hole concentration of the NiO layer decreases. Surface treatment using solutions or a plasma process is also a practical method to remove the defects at the β-Ga$_2$O$_3$ surface and realize a high-quality hetero-interface.

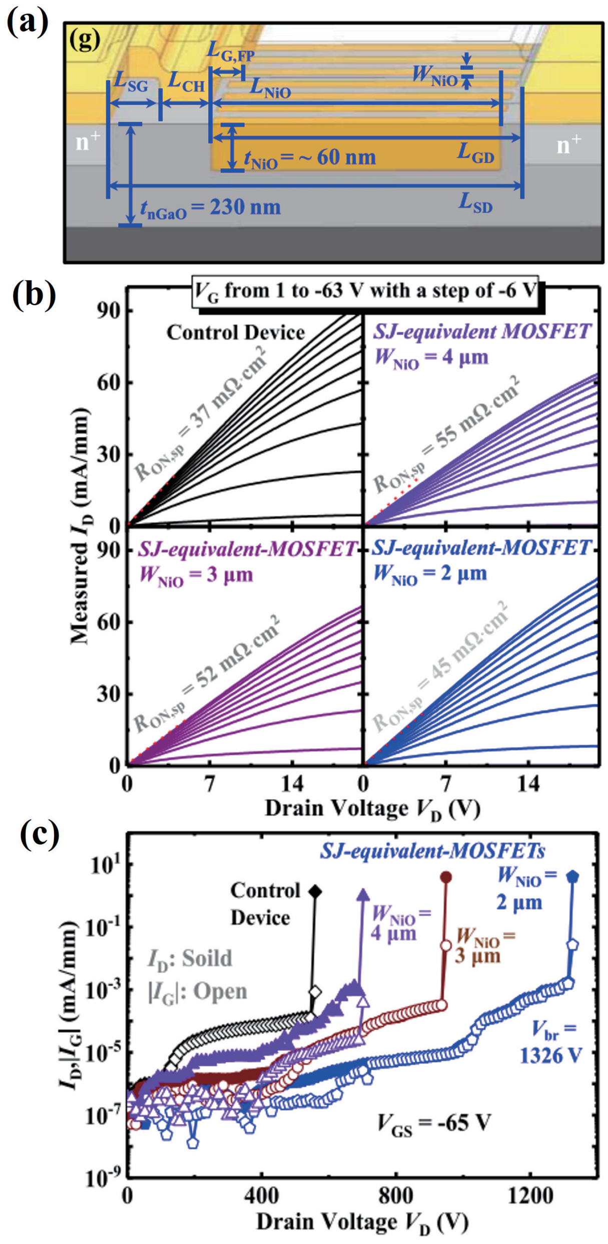

Fig. 21. (Color online) (a) 3-D schematic of the fabricated β-Ga$_2$O$_3$ SJ-equivalent MOSFET. (b) Measured I_D–V_D curves of the devices. (c) Reverse *I*–*V* characteristics of the devices. Reproduced from Ref. [35]. Copyright 2022, IEEE.

Device reliability is very important for the commercial application of the NiO/β-Ga$_2$O$_3$ heterojunction power devices, especially at high temperatures. The sputtered NiO layer usually faces a thermal stability issue, whose hole concentration usually reduces at high temperatures. The reliability verifications for the NiO/β-Ga$_2$O$_3$ heterojunction devices are still lacking and awaiting future exploration.

Acknowledgements

This work was supported by the Guangdong Basic and Applied Basic Research Foundation under Grant No. 2022A1515012163.

References

[1] She X, Huang A Q, Lucía Ó, et al. Review of silicon carbide power devices and their applications. IEEE Trans Ind Electron, 2017, 64, 8193

[2] Jones E A, Wang F F, Costinett D. Review of commercial GaN power devices and GaN-based converter design challenges. IEEE J Emerg Sel Top Power Electron, 2016, 4, 707

[3] Saikumar A K, Nehate S D, Sundaram K B. Review—RF sputtered films of Ga_2O_3. ECS J Solid State Sci Technol, 2019, 8, Q3064

[4] Pearton S J, Yang J C, Cary P H, et al. A review of Ga_2O_3 materials, processing, and devices. Appl Phys Rev, 2018, 5, 011301

[5] Zhou H, Zhang J C, Zhang C F, et al. A review of the most recent progresses of state-of-art gallium oxide power devices. J Semicond, 2019, 40, 011803

[6] Yoshioka S, Hayashi H, Kuwabara A, et al. Structures and energetics of Ga_2O_3 polymorphs. J Phys: Condens Matter, 2007, 19, 346211

[7] Víllora E G, Shimamura K, Yoshikawa Y, et al. Large-size β-Ga_2O_3 single crystals and wafers. J Cryst Growth, 2004, 270, 420

[8] Kuramata A, Koshi K, Watanabe S, et al. High-quality β-Ga_2O_3 single crystals grown by edge-defined film-fed growth. Jpn J Appl Phys, 2016, 55, 1202A2

[9] Alema F, Zhang Y W, Osinsky A, et al. Low temperature electron mobility exceeding 10^4 cm^2/V s in MOCVD grown β-Ga_2O_3. APL Mater, 2019, 7, 121110

[10] Zhang Y W, Alema F, Mauze A, et al. MOCVD grown epitaxial β-Ga_2O_3 thin film with an electron mobility of 176 cm^2/V s at room temperature. APL Mater, 2018, 7, 022506

[11] Chen Y P, Xia X C, Liang H W, et al. Growth pressure controlled nucleation epitaxy of pure phase ε- and β-Ga_2O_3 films on Al_2O_3 via metal–organic chemical vapor deposition. Cryst Growth Des, 2018, 18, 1147

[12] Kukushkin S A, Nikolaev V I, Osipov A V, et al. Epitaxial gallium oxide on a SiC/Si substrate. Phys Solid State, 2016, 58, 1876

[13] Wei H L, Chen Z W, Wu Z P, et al. Epitaxial growth and characterization of $CuGa_2O_4$ films by laser molecular beam epitaxy. AIP Adv, 2017, 7, 115216

[14] Sasaki K, Higashiwaki M, Kuramata A, et al. MBE grown Ga_2O_3 and its power device applications. J Cryst Growth, 2013, 378, 591

[15] Joishi C, Rafique S, Xia Z B, et al. Low-pressure CVD-grown β-Ga_2O_3 bevel-field-plated Schottky barrier diodes. Appl Phys Express, 2018, 11, 031101

[16] Baldini M, Albrecht M, Fiedler A, et al. Si- and Sn-doped homoepitaxial β-Ga_2O_3 layers grown by MOVPE on (010)-oriented substrates. ECS J Solid State Sci Technol, 2016, 6, Q3040

[17] Varley J B, Janotti A, Franchini C, et al. Role of self-trapping in luminescence and p-type conductivity of wide-band-gap oxides. Phys Rev B, 2012, 85, 081109

[18] Lyons J L. A survey of acceptor dopants for β. Semicond Sci Technol, 2018, 33, 05LT02

[19] Yang J C, Xian M H, Carey P, et al. Vertical geometry 33.2 A, 4.8 MW cm^2 Ga_2O_3 field-plated Schottky rectifier arrays. Appl Phys Lett, 2019, 114, 232106

[20] Zhou H, Yan Q L, Zhang J C, et al. High-performance vertical β-Ga_2O_3 Schottky barrier diode with implanted edge termination. IEEE Electron Device Lett, 2019, 40, 1788

[21] Li W S, Nomoto K, Hu Z Y, et al. Field-plated Ga_2O_3 trench Schottky barrier diodes with a $BV_2/R_{on,\ sp}$ of up to 0.95 GW/cm^2. IEEE Electron Device Lett, 2020, 41, 107

[22] Jian Z A, Mohanty S, Ahmadi E. Switching performance analysis of 3.5 kV Ga_2O_3 power FinFETs. IEEE Trans Electron Devices, 2021, 68, 672

[23] Nakagomi S, Hiratsuka K, Kakuda Y, et al. Beta-gallium oxide/SiC heterojunction diodes with high rectification ratios. ECS J Solid State Sci Technol, 2016, 6, Q3030

[24] Zhang Y C, Li Y F, Wang Z Z, et al. Investigation of β-Ga_2O_3 films and β-Ga_2O_3/GaN heterostructures grown by metal organic chemical vapor deposition. Sci China Phys Mech Astron, 2020, 63, 117311

[25] Wang Y G, Gong H H, Lv Y J, et al. 2.41 kV vertical P-NiO/n-Ga_2O_3 heterojunction diodes with a record Baliga's figure-of-merit of 5.18 GW/cm^2. IEEE Trans Power Electron, 2022, 37, 3743

[26] Kokubun Y, Kubo S, Nakagomi S. All-oxide p–n heterojunction diodes comprising p-type NiO and n-type β-Ga_2O_3. Appl Phys Express, 2016, 9, 091101

[27] Lu X, Zhou X D, Jiang H X, et al. 1-kV sputtered p-NiO/n-Ga_2O_3 heterojunction diodes with an ultra-low leakage current below 1 μA/cm^2. IEEE Electron Device Lett, 2020, 41, 449

[28] Watahiki T, Yuda Y, Furukawa A, et al. Heterojunction p-Cu_2O/n-Ga_2O_3 diode with high breakdown voltage. Appl Phys Lett, 2017, 111, 222104

[29] Budde M, Splith D, Mazzolini P, et al. SnO/β-Ga_2O_3 vertical pn heterojunction diodes. Appl Phys Lett, 2020, 117, 252106

[30] Gallagher J C, Koehler A D, Tadjer M J, et al. Demonstration of CuI as a P–N heterojunction to β. Appl Phys Express, 2019, 12, 104005

[31] Chen H L, Lu Y M, Hwang W S. Characterization of sputtered NiO thin films. Surf Coat Technol, 2005, 198, 138

[32] Lv Y J, Wang Y G, Fu X C, et al. Demonstration of β-Ga_2O_3 junction barrier Schottky diodes with a Baliga's figure of merit of 0.85 GW/cm^2 or a 5A/700 V handling capabilities. IEEE Trans Power Electron, 2021, 36, 6179

[33] Wang C L, Gong H H, Lei W N, et al. Demonstration of the p-NiO_x/n-Ga_2O_3 heterojunction gate FETs and diodes with $BV^2/R_{on,\ sp}$ figures of merit of 0.39 GW/cm^2 and 1.38 GW/cm^2. IEEE Electron Device Lett, 2021, 42, 485

[34] Yan Q L, Gong H H, Zhou H, et al. Low density of interface trap states and temperature dependence study of Ga_2O_3 Schottky barrier diode with p-NiO_x termination. Appl Phys Lett, 2022, 120, 092106

[35] Wang Y B, Gong H H, Jia X L, et al. Demonstration of β-Ga_2O_3 superjunction-equivalent MOSFETs. IEEE Trans Electron Devices, 2022, 69, 2203

[36] Wang Y, Qin Q Z. A nanocrystalline NiO thin-film electrode prepared by pulsed laser ablation for Li-ion batteries. J Electrochem Soc, 2002, 149, A873

[37] Jlassi M, Sta I, Hajji M, et al. Optical and electrical properties of nickel oxide thin films synthesized by sol–gel spin coating. Mater Sci Semicond Process, 2014, 21, 7

[38] Park J H, Seo J, Park S, et al. Efficient $CH_3NH_3PbI_3$ perovskite solar cells employing nanostructured p-type NiO electrode formed by a pulsed laser deposition. Adv Mater, 2015, 27, 4013

[39] Hotový I, Búc D, Haščík Š, et al. Characterization of NiO thin films deposited by reactive sputtering. Vacuum, 1998, 50, 41

[40] Budde M, Remmele T, Tschammer C, et al. Plasma-assisted molecular beam epitaxy of NiO on GaN(00.1). J Appl Phys, 2020, 127, 015306

[41] Tadjer M J, Luna L E, Cleveland E, et al. Fabrication and characterization of β-Ga_2O_3 heterojunction rectifiers. ECS Trans, 2018, 85, 21

[42] Hajakbari F. Characterization of nanocrystalline nickel oxide thin films prepared at different thermal oxidation temperatures. J Nanostruct Chem, 2020, 10, 97

[43] Pintor-Monroy M I, Barrera D, Murillo-Borjas B L, et al. Tunable electrical and optical properties of nickel oxide (NiO_x) thin films for fully transparent NiO_x-Ga_2O_3 p-n junction diodes. ACS Appl Mater Interfaces, 2018, 10, 38159

[44] Schlupp P, Splith D, von Wenckstern H, et al. Electrical properties of vertical p-NiO/n-Ga_2O_3 and p-$ZnCo_2O_4$/n-Ga_2O_3 pn-heterodiodes. Phys Status Solidi A, 2019, 216, 1800729

[45] Zhang J Y, Han S B, Cui M Y, et al. Fabrication and interfacial electronic structure of wide bandgap NiO and Ga_2O_3 p–n heterojunction. ACS Appl Electron Mater, 2020, 2, 456

[46] Li K H, Alfaraj N, Kang C H, et al. Deep-ultraviolet photodetection using single-crystalline β-Ga_2O_3/NiO heterojunctions. ACS Appl

Mater Interfaces, 2019, 11, 35095

[47] Deng Y X, Yang Z Q, Xu T L, et al. Band alignment and electrical properties of NiO/β-Ga_2O_3 heterojunctions with different β-Ga_2O_3 orientations. Appl Surf Sci, 2023, 622, 156917

[48] Luo H X, Zhou X D, Chen Z M, et al. Fabrication and characterization of high-voltage NiO/β-Ga_2O_3 heterojunction power diodes. IEEE Trans Electron Devices, 2021, 68, 3991

[49] Liao C, Lu X, Xu T L, et al. Optimization of NiO/β-Ga_2O_3 heterojunction diodes for high-power application. IEEE Trans Electron Devices, 2022, 69, 5722

[50] Gong H H, Chen X H, Xu Y, et al. Band alignment and interface recombination in NiO/β-Ga_2O_3 type-II p-n heterojunctions. IEEE Trans Electron Devices, 2020, 67, 3341

[51] Guo Z, Verma A, Wu X F, et al. Anisotropic thermal conductivity in single crystal β-gallium oxide. Appl Phys Lett, 2015, 106, 111909

[52] Wong M H, Sasaki K, Kuramata A, et al. Electron channel mobility in silicon-doped Ga_2O_3 MOSFETs with a resistive buffer layer. Jpn J Appl Phys, 2016, 55, 1202B9

[53] Jang S, Jung S, Beers K, et al. A comparative study of wet etching and contacts on $(\bar{2}01)$ and (010) oriented β-Ga_2O_3. J Alloys Compd, 2018, 731, 118

[54] Zhang K, Xu Z W, Zhao J L, et al. Anisotropies of angle-resolved polarized Raman response identifying in low miller index β-Ga_2O_3 single crystal. Appl Surf Sci, 2022, 581, 152426

[55] Yatskiv R, Tiagulskyi S, Grym J. Influence of crystallographic orientation on Schottky barrier formation in gallium oxide. J Electron Mater, 2020, 49, 5133

[56] Fu H Q, Chen H, Huang X Q, et al. A comparative study on the electrical properties of vertical $(\bar{2}01)$ and (010) β-Ga_2O_3 Schottky barrier diodes on EFG single-crystal substrates. IEEE Trans Electron Devices, 2018, 65, 3507

[57] Xia X Y, Li J S, Chiang C C, et al. Annealing temperature dependence of band alignment of NiO/β-Ga_2O_3. J Phys D: Appl Phys, 2022, 55, 385105

[58] Wang Z P, Gong H H, Meng C X, et al. Majority and minority carrier traps in NiO/β-Ga_2O_3 p-n heterojunction diode. IEEE Trans Electron Devices, 2022, 69, 981

[59] Grundmann M, Karsthof R, von Wenckstern H. Interface recombination current in type II heterostructure bipolar diodes. ACS Appl Mater Interfaces, 2014, 6, 14785

[60] Riben A R, Feucht D L. Electrical transport in nGe-pGaAs heterojunctions. Int J Electron, 1966, 20, 583

[61] Riben A R, Feucht D L. nGe–pGaAs heterojunctions. Solid State Electron, 1966, 9, 1055

[62] Zhang J C, Dong P F, Dang K, et al. Ultra-wide bandgap semiconductor Ga_2O_3 power diodes. Nat Commun, 2022, 13, 3900

[63] Wang Z P, Gong H H, Yu X X, et al. Trap-mediated bipolar charge transport in NiO/Ga_2O_3 p^+-n heterojunction power diodes. Sci China Mater, 2022, 66, 1157

[64] Zimmermann C, Frodason Y K, Barnard A W, et al. Ti- and Fe-related charge transition levels in β-Ga_2O_3. Appl Phys Lett, 2020, 116, 072101

[65] Ingebrigtsen M E, Varley J B, Kuznetsov A Y, et al. Iron and intrinsic deep level states in Ga_2O_3. Appl Phys Lett, 2018, 112, 042104

[66] Hao W B, He Q M, Zhou K, et al. Low defect density and small I – V curve hysteresis in NiO/β-Ga_2O_3 pn diode with a high PFOM of 0.65 GW/cm^2. Appl Phys Lett, 2021, 118, 043501

[67] Gong H H, Yu X X, Xu Y, et al. Vertical field-plated NiO/Ga_2O_3 heterojunction power diodes. 2021 5th IEEE Electron Devices Technology & Manufacturing Conference (EDTM), 2021, 1

[68] Gong H H, Chen X H, Xu Y, et al. A 1.86-kV double-layered NiO/β-Ga_2O_3 vertical p–n heterojunction diode. Appl Phys Lett, 2020, 117, 022104

[69] Li J S, Chiang C C, Xia X Y, et al. Demonstration of 4.7 kV breakdown voltage in NiO/β-Ga_2O_3 vertical rectifiers. Appl Phys Lett, 2022, 121, 042105

[70] Zhou F, Gong H H, Wang Z P, et al. Over 1.8 GW/cm^2 beveled-mesa NiO/β-Ga_2O_3 heterojunction diode with 800 V/10 A nanosecond switching capability. Appl Phys Lett, 2021, 119, 262103

[71] Gong H H, Yu X X, Xu Y, et al. β-Ga_2O_3 vertical heterojunction barrier Schottky diodes terminated with p-NiO field limiting rings. Appl Phys Lett, 2021, 118, 202102

[72] De Santi C, Fregolent M, Buffolo M, et al. Carrier capture kinetics, deep levels, and isolation properties of β-Ga_2O_3 Schottky-barrier diodes damaged by nitrogen implantation. Appl Phys Lett, 2020, 117, 262108

[73] Yan Q L, Gong H H, Zhang J C, et al. β-Ga_2O_3 hetero-junction barrier Schottky diode with reverse leakage current modulation and $BV^2/R_{on,sp}$ value of 0.93 GW/cm^2. Appl Phys Lett, 2021, 118, 122102

[74] Polyakov A Y, Lee I H, Smirnov N B, et al. Defects at the surface of β-Ga_2O_3 produced by Ar plasma exposure. APL Mater, 2019, 7, 061102

[75] Alfieri G, Mihaila A, Godignon P, et al. Deep level study of chlorine-based dry etched β-Ga_2O_3. J Appl Phys, 2021, 130, 025701

[76] Lu X, Xu T L, Deng Y X, et al. Performance-enhanced NiO/β-Ga_2O_3 heterojunction diodes fabricated on an etched β-Ga_2O_3 surface. Appl Surf Sci, 2022, 597, 153587

[77] Lv Y J, Zhou X Y, Long S B, et al. Lateral source field-plated β-Ga_2O_3 MOSFET with recorded breakdown voltage of 2360 V and low specific on-resistance of 560 mΩ cm^2. Semicond Sci Technol, 2019, 34, 11LT02

[78] Mun J K, Cho K, Chang W, et al. Editors' choice—2.32 kV breakdown voltage lateral β-Ga_2O_3 MOSFETs with source-connected field plate. ECS J Solid State Sci Technol, 2019, 8, Q3079

[79] Tetzner K, Bahat Treidel E, Hilt O, et al. Lateral 1.8 kV β-Ga_2O_3 MOSFET with 155 MW/cm^2 power figure of merit. IEEE Electron Device Lett, 2019, 40, 1503

[80] Lv Y J, Liu H Y, Zhou X Y, et al. Lateral β-Ga_2O_3 MOSFETs with high power figure of merit of 277 MW/cm^2. IEEE Electron Device Lett, 2020, 41, 537

[81] Zhou X Z, Liu Q, Hao W B, et al. Normally-off β-Ga_2O_3 power heterojunction field-effect-transistor realized by p-NiO and recessed-gate. 2022 IEEE 34th International Symposium on Power Semiconductor Devices and ICs (ISPSD), 2022, 101

[82] Konishi K, Goto K, Murakami H, et al. 1-kV vertical Ga_2O_3 field-plated Schottky barrier diodes. Appl Phys Lett, 2017, 110, 103506

[83] Zhang Y N, Zhang J C, Feng Z Q, et al. Impact of implanted edge termination on vertical β-Ga_2O_3 Schottky barrier diodes under OFF-state stressing. IEEE Trans Electron Devices, 2020, 67, 3948

[84] Gao Y Y, Li A, Feng Q, et al. High-voltage β-Ga_2O_3 Schottky diode with argon-implanted edge termination. Nanoscale Res Lett, 2019, 14, 8

[85] Wang Y G, Lv Y J, Long S B, et al. High-voltage (-201) β-Ga_2O_3 vertical Schottky barrier diode with thermally-oxidized termination. IEEE Electron Device Lett, 2020, 41, 131

[86] Hirao T, Onose H, Kan Y S, et al. Edge termination with enhanced field-limiting rings insensitive to surface charge for high-voltage SiC power devices. IEEE Trans Electron Devices, 2020, 67, 2850

[87] Fujihira T. Theory of semiconductor superjunction devices. Jpn J Appl Phys, 1997, 36, 6254

[88] Deboy G, Marz N, Stengl J P, et al. A new generation of high voltage MOSFETs breaks the limit line of silicon. International Electron Devices Meeting, 1998, 683

[89] Lorenz L, Deboy G, Knapp A, et al. COOLMOS/sup TM/-a new milestone in high voltage power MOS. 11th International Symposium on Power Semiconductor Devices and ICs, 1999, 3

[90] Udrea F, Deboy G, Fujihira T. Superjunction power devices, history, development, and future prospects. IEEE Trans Electron

Devices, 2017, 64, 713

[91] Nassif-Khalil S G, Salama C A T. Super-junction LDMOST on a silicon-on-sapphire substrate. IEEE Trans Electron Devices, 2003, 50, 1385

[92] Duan B X, Cao Z, Yuan X, et al. New superjunction LDMOS breaking silicon limit by electric field modulation of buffered step doping. IEEE Electron Device Lett, 2015, 36, 47

[93] Xiao M, Zhang R Z, Dong D, et al. Design and simulation of GaN superjunction transistors with 2-DEG channels and fin channels. IEEE J Emerg Sel Top Power Electron, 2019, 7, 1475

[94] Zhong X Q, Wang B Z, Wang J, et al. Experimental demonstration and analysis of a 1.35-kV 0.92-m Ω·cm^2 SiC superjunction Schottky diode. IEEE Trans Electron Devices, 2018, 65, 1458

[95] Nakajima A, Sumida Y, Dhyani M H, et al. GaN-based super heterojunction field effect transistors using the polarization junction concept. IEEE Electron Device Lett, 2011, 32, 542

[96] Wang H, Napoli E, Udrea F. Breakdown voltage for superjunction power devices with charge imbalance: An analytical model valid for both punch through and non punch through devices. IEEE Trans Electron Devices, 2009, 56, 3175

Xing Lu received the B.S. degree from Fudan University, Shanghai, China, and the Ph.D. degree from The Hong Kong University of Science and Technology, Hong Kong. He is currently an Associate Professor with the State Key Laboratory of Optoelectronic Materials and Technologies, School of Electronics and Information Technology, Sun Yat-sen University, Guangzhou, China.

Gang Wang received the B.S. degree from Jilin University, Changchun, China, and the Ph.D. degree from Nagoya Institute of Technology, Japan. He is currently a Professor with the State Key Laboratory of Optoelectronic Materials and Technologies, School of Electronics and Information Technology, Sun Yat-sen University, Guangzhou, China.